Surface & Coatings Technology 326 (2017) 1–10

Contents lists available at ScienceDirect

Surface & Coatings Technology

journal homepage: www.elsevier.com/locate/surfcoat

Effects of suspension properties on the microstructure of Al_2O_3 coatings deposited onto macroporous SiC substrate

Takamasa Mori *, Saori Yamada, Naoya Iwata

Department of Chemical Science and Technology, Faculty of Bioscience and Applied Chemistry, Hosei University, 3-7-2 Kajino-cho, Koganei, Tokyo 184-8584, Japan

ARTICLE INFO

Article history:
Received 3 May 2017
Revised 14 July 2017
Accepted in revised form 15 July 2017
Available online 16 July 2017

Keywords:
Spin coating
Catalyst supporting particle
Porous substrate
Suspension
Particle dispersion
Air permeation resistance

ABSTRACT

In this paper the effects of the suspension preparation conditions on suspension coating of porous substrates were investigated. Alumina suspensions were prepared using varying types of additives, including non-ionic polyethylene glycol (PEG), cationic polyethylene imine (PEI), and anionic sodium carboxymethyl cellulose (CMC). Prepared suspensions were coated on porous SiC substrates by spin coating. The flow curves of the suspensions were measured, whereas their particle dispersion states were also observed directly using an optical microscope. In addition, the surface and cross-section of each coating were observed by SEM and analysed by EDX. Finally, the air permeability of each coating was measured.

For the suspension with PEG, alumina particles dispersed well in the suspension and the added PEG formed a network structure, resulting in a homogeneous coating on the surface of the substrate with less particle penetration into the substrate pores. For the suspension with CMC and the suspension with PEI, since particles flocculated in the suspensions, particle penetration into the substrate pores hardly occurred, however, the formed coating was inhomogeneous.

1. Introduction

Recently, porous ceramic materials have been widely used in various industries such as hot gas separation [1], direct methanol fuel cell [2], carbon dioxide capture and storage [3], particulate filters for diesel engines [4], and waste water treatment [5] industries. As such, much research related to porous ceramics has already been conducted. For practical use, a fine catalyst or catalyst-supporting powder is coated on the surface of porous ceramic substrates. The state of this coating on the substrate affects its performance. For example, if the fine particles form aggregates, the catalysis reaction efficiency decreases; if the fine particles penetrate into the pores of the substrate, the fluid permeation resistance increases. Therefore, the coating state, including the distribution of fine particles on and in porous substrates, needs to be controlled.

One of the coating techniques is dip coating of porous substrates into suspensions in which fine particles are dispersed in an appropriate medium. Usually these fine particles are dispersed in a medium with a dispersant and a binder, and dipping of the porous substrate into the prepared suspension is followed by drying and heating to immobilize the particles. Compared to coatings on glass or metal substrates with relatively smooth surfaces, few papers exist on coatings of fine particles on porous substrates. Paunovic et al. reported about silica coating on porous substrates [6]. Zhang et al. achieved a silicon coating on porous Si_3N_4 [7]. Agrafiotis et al. have coated a ceria-doped alumina on ceramic honeycombs [8]. Itoh et al. have coated $Ca(Ti,Fe)O_3$ on porous substrates [9]. Zwinkels et al. have described ceramic coatings on metal substrates [10]. However, the optimal properties of suspensions used for coating of porous substrates have not been identified yet, because these substrates often have relatively uneven surfaces and pore sizes that are larger than the size of fine catalytic particles. In addition, the desirable structure of fine particles coated on substrates varies by final product; thus, control of the structure is needed to be able to freely fabricate coatings with different structures. In previous papers on dip coating of porous substrates, mainly the apparent viscosity was investigated in order to optimize the slurry conditions for alumina coatings [11,12], Cu/Mn/ZnO catalyst coatings [13], γ-alumina coatings [14], and yttria-stabilized-zirconia coatings [15], while other suspension properties related to the particle dispersion state were not discussed. It was also reported that, in some cases, the apparent viscosity did not correspond well with the particle packing ability of a suspension [16–20], an important observation since the apparent viscosity is one of the most important parameters for the coating process. Therefore, further investigation of suspension properties is necessary to establish optimal suspension preparation guidelines to control the coating state. In this paper, the relationship between the suspension properties and the microstructure of coatings on porous substrates was examined by changing the type of suspension

* Corresponding author.
E-mail address: tmori@hosei.ac.jp (T. Mori).

http://dx.doi.org/10.1016/j.surfcoat.2017.07.036
0257-8972/

Nomenclatures

k	Viscosity constant in Eq. (1) [Pa•s^n]
n	viscosity index in Eq. (1) [−]
$\dot{\gamma}$	shear rate for flow curve measurement [s^{-1}]
τ	shear stress for flow curve measurement [Pa]
τ_c	yield stress (intercept of flow curve) [Pa]
ε_0	permittivity of free space [F•m^{-1}]
ε_r	relative permittivity [−]
ξ	zeta potential of particle [V]
u_{ave}	average particle mobility for electrophoresis [m^2•V^{-1}•s^{-2}]
μ	medium viscosity [Pa•s]
Φ	final volume fraction of formed sediment [−]
H	final height of formed sediment [m]
ϕ	initial volume fraction of slurry for settling test [−]
h	initial height of slurry for settling test [m]

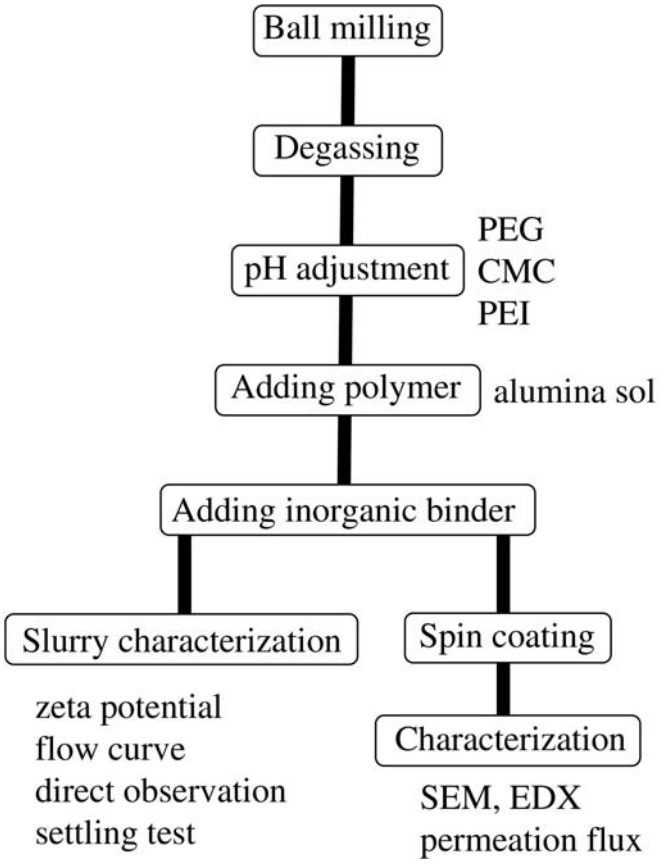

Fig. 1. Experimental flow.

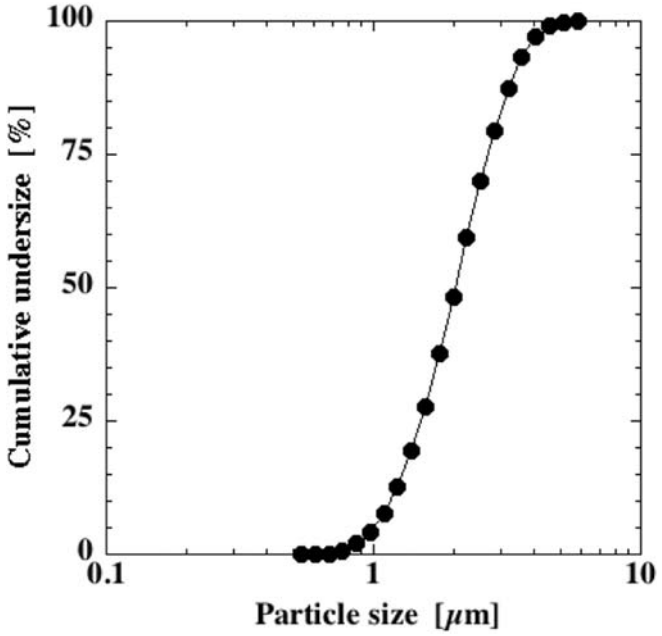

Fig. 2. Particle size distribution of alumina powder used in this study.

additives. For suspension characterization, not only apparent viscosity measurements, but also sedimentation tests were conducted. In addition, direct observations of particle dispersion and flocculation [21,22] were made. All results were analysed with regards to the final coating properties.

2. Experiment

Fig. 1 shows the experimental flow. In brief, experiments consisted of four parts: suspension preparation, suspension characterization, substrate coating, and coating characterization. Details of each aspect are described below.

2.1. Suspension preparation

An alumina powder with an average particle size of 1.98 μm was used as a model catalyst-supporting powder particle. The particle density, measured by pycnometry, was 2480 kg·m^{-3}. The alumina powder was mixed with deionized water to prepare a suspension with a particle concentration of 2.0 vol%. The prepared suspension was ball-milled for 4 h in a polyethylene pot with 1.5-mm-diameter zirconia beads. Fig. 2 shows the particle size distribution of the alumina powder after ball milling, measured by a laser diffraction particle size analyser (SALD-3100, Shimadzu Corporation). Subsequently, the suspension was degassed and its pH value adjusted to approximately 5.0 with 1 M HCl. An additive aqueous solution that was prepared in advance was then added to the suspension while stirring. The added amount was 2.4 wt% of the mass of the alumina powder in the suspension. The additives used in this study were the non-ionic polymer polyethylene glycol (PEG; M_w = 2000,000, Wako Pure Chemical Industries), the cationic polymer polyethylenimine (PEI; M_w = 70,000, Wako Pure Chemical

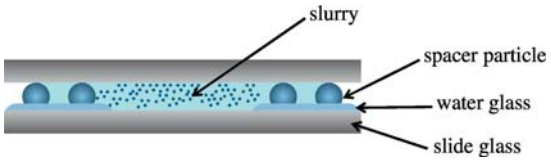

Fig. 3. Schematic illustration of sample configuration for direct observation of suspensions.

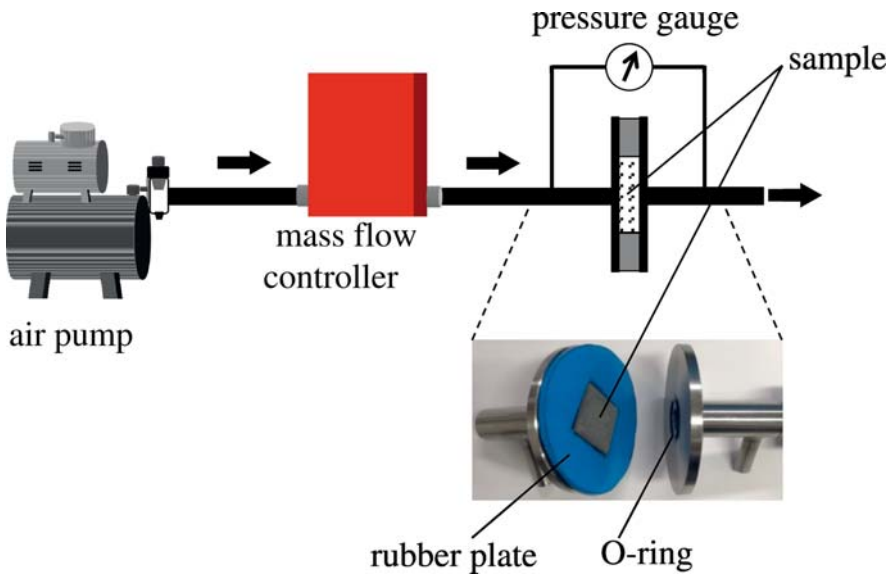

Fig. 4. Schematic illustration of air permeation test equipment.

Industries), and the anionic polymer sodium carboxymethyl cellulose (CMC; M_w = 100,000, Tokyo Chemical Industry Co., Ltd.). Finally, an alumina aqueous sol, in which alumina hydrate particles with a pseudo-boehmite structure were dispersed, was added to the suspension as an inorganic binder. The solid concentration of the alumina sol in the suspension was 0.48 wt%. Here, the pH of the prepared slurry changed from an initial pH of 5.0 due to the added polymers. However, another pH adjustment was not done.

2.2. Suspension characterization

2.2.1. Flow curve measurements

Each prepared suspension was poured into a cup of a coaxial double-cylinder rotation viscometer (Rheolab QC, Anton Paar) and the shear stress acting on the rotor was measured by changing the shear rate from 0 to 2000 s^{-1}. Obtained flow curves, i.e., the shear stress τ vs. shear rate $\dot{\gamma}$, were fitted with the following power-law model [23,24] to determine the yield stress, τ_c:

$$\tau = \tau_c + k\dot{\gamma}^n \tag{1}$$

where k and n are constants. The apparent viscosities at a shear rate of 1500 s^{-1} were also determined from the flow curves.

2.2.2. Sedimentation test

Ten milliliter of each prepared suspension was poured in a test tube and centrifuged at 4200 rpm (corresponding to a centrifugal acceleration of 2370 G). We visually inspected the position of the interface between the supernatant and the suspension or sediment until it remained constant after at least one additional day of centrifugation. The final height H of each formed sediment was measured, calculating the final packing fraction of the sediment Φ by the following mass balance equation.

$$\Phi = \frac{\phi h}{H} \tag{2}$$

where ϕ is the initial particle concentration and h is the initial height of the suspension.

2.2.3. Direct observation of particle dispersion state

Some spacer particles with a particle size of 30 μm (Micropearl, Sekisui Chemical Co. Ltd.) were placed on a commercial glass slide and

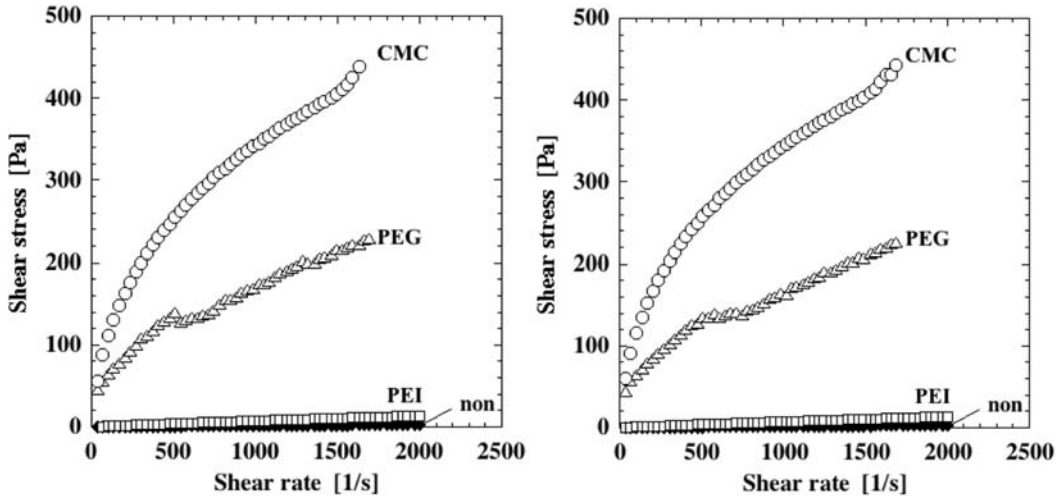

Fig. 5. Flow curves of the prepared suspensions without (a) and with inorganic binder (b).

Table 1
Apparent viscosity at 1500 s^{-1} and yield stress.

Additive	Apparent viscosity [Pa•s]	Yield stress [Pa]
CMC	0.269	15.0
PEG	0.139	37.0
PEI	0.007	0.0
non	0.001	0.0

fixed by water glass (Wako Pure Chemical Industries). Another glass slide was placed on top and rubbed to ensure that the spacer particles did not pile up before the water glass had dried. The glass slide with the spacer particles fixed by water glass was dried for 5 h at 120 °C; this is called the base glass.

Samples for direct observation of the particle dispersion state were prepared by sandwiching prepared suspensions between the base glass and another glass slide. The edge of each prepared sample was sealed with a paraffin jelly to prevent a concentration change of the suspension due to evaporation. Fig. 3 shows a schematic illustration of each sample for direct observation of the particle dispersion state.

Prepared samples were observed through an optical microscope (BX60, Olympus Corporation) in transmission mode. Five photos of each suspension were taken, changing the visual field for each. Photos were analysed by the free software package ImageJ to determine the average particle or flocculation size. Each photo was binarised, after which the linear intercept lengths of particles were measured by drawing a horizontal line in the binarised photo. By scanning from the top to the bottom of the photo, we could thus obtain the linear intercept length distribution and average particle or flocculation size.

2.2.4. Zeta potential measurements

The zeta potential of the alumina particles before and after the addition of the additives was measured by electrophoresis. A small amount of raw alumina powder or sampled alumina powder from each suspension was dispersed in deionized water with the use of an ultrasonic homogenizer. Then, the prepared suspensions were divided in equal parts and their pH values controlled to a certain value through the addition of HCl and NaOH. Subsequently, the zeta potential of the powder was measured using a Model 502 (Nihon Rufuto Co. Ltd.). The particle velocity was measured under an applied DC current of 45 V. Considering the effect of polarization of the materials in the suspension, as well as the change in pH, each measurement was repeated 10 times while changing the positive and negative electrodes. From the average measured particle velocity, the zeta potential was calculated using Smoluchowski's equation [25]:

$$\xi = \frac{\mu u_{ave}}{\varepsilon_0 \varepsilon} \tag{3}$$

Where ξ is the zeta potential, ε is the electrical permittivity of a vacuum, ε_0 is the dielectric constant, u_{ave} is the average velocity, and μ is the solution viscosity.

2.3. Coating

Each prepared suspension was spin-coated on a porous substrate using a spin coater. The porous substrate used in this study was a porous SiC plate with a size of 20 mm × 20 mm × 1.0 mm (AZPS-40, pore size ~5–30 μm, porosity 30%, Asuzac Inc.). The SiC substrates were washed in an ultrasonic bath for 3 min and then heated at 900 °C for 4 h for advance surface hydrophilisation. Then, 0.5 g of each prepared suspension was dropped on a porous substrate, and the substrate was rotated at 200 rpm for 20 s and 2000 rpm for 30 s. Finally, the coated substrates were dried at room temperature.

2.4. Coating characterization

The coated and dried substrates were heated at 700 °C for 7 h. After heating, the surfaces and cross-sections of samples were observed by scanning electron microscopy (SEM) and analysed by energy-dispersive x-ray spectroscopy (EDX), focusing on Si and Al. For EDX analysis of the cross-sections, the area between the surface and 600 μm below the surface was divided into four parts, and the mass ratio of Al/Si in each part was determined.

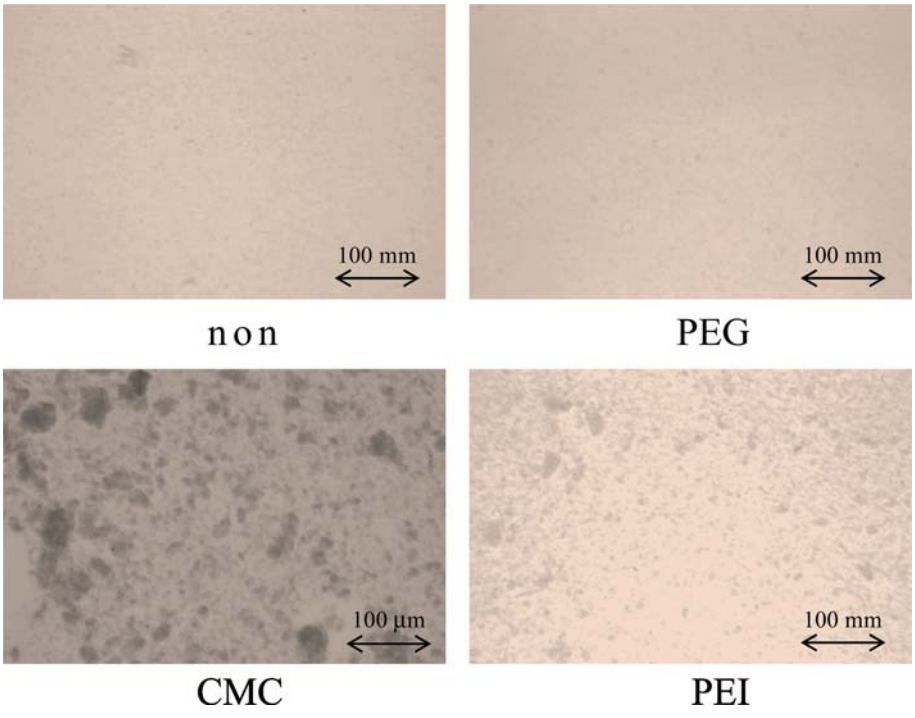

Fig. 6. Direct observation of suspensions without inorganic binder.

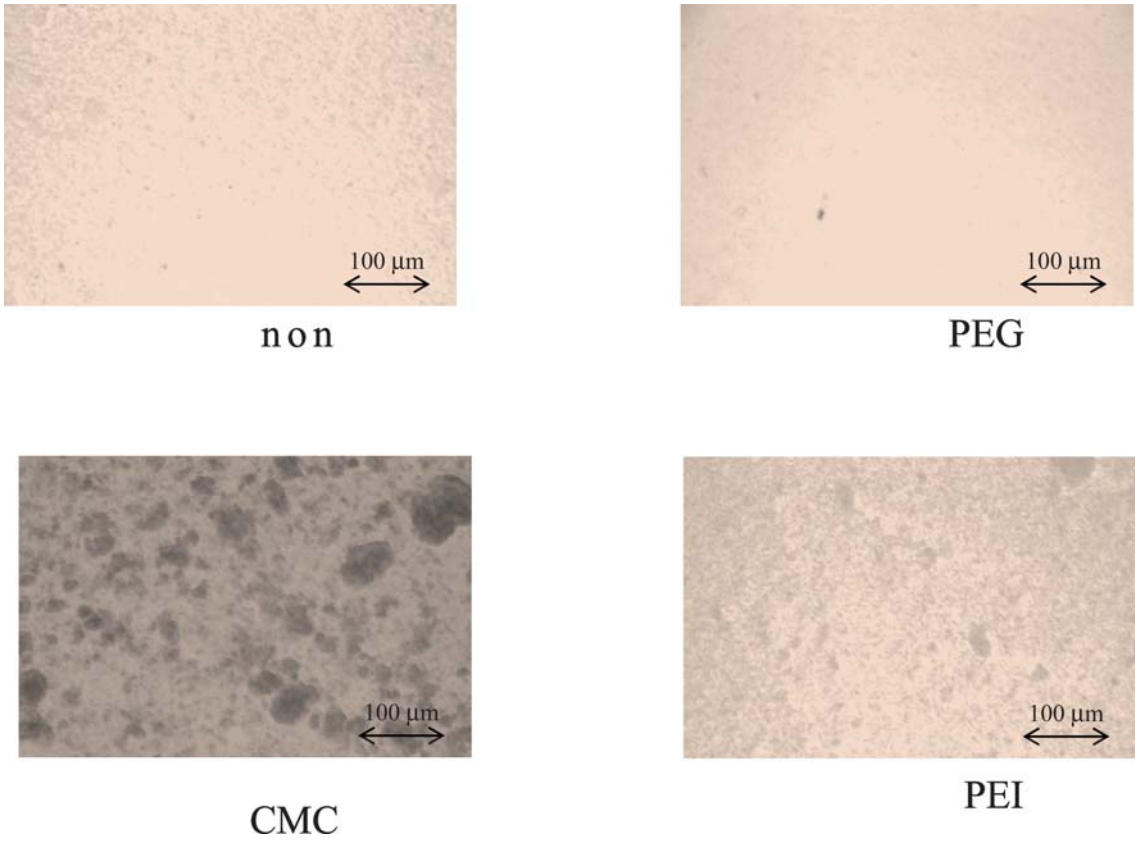

Fig. 7. Direct observation of suspensions with inorganic binder.

In addition, the air permeability for the pristine and coated porous substrates was measured by the apparatus illustrated in Fig. 4. The pressure difference between both sides of the substrate was measured by a pressure gauge at a constant flow rate of 200 mL/min. Considering the variation in permeability between the raw substrates, we will discuss the increase in ratio of the permeation resistance before and after coating.

3. Results and discussion

3.1. Suspension characterization

Fig. 5 shows the flow curves of suspensions with and without the inorganic binder. The flow curves were compared since the inorganic binder may influence the dispersion state of alumina particles in suspensions, even though its role was only to immobilize the alumina particles after drying and heating. Nonetheless, the flow curve hardly changed before and after addition of the inorganic binder. The yield stress, determined by curve fitting of the flow curve by Eq. (1), and apparent viscosity values at a shear rate of 1500 s^{-1} are summarized in Table 1. The suspensions with CMC and PEG exhibited yield stresses and relatively high apparent viscosities, while the suspensions with PEI and without any additives did not exhibit yield stresses and quite low apparent viscosities. Fig. 6 and 7 show the photos of suspensions directly observed as described above. The average particle sizes, determined from the photos by image analysis, are summarized in Table 2. The particles in the suspension with CMC flocculated, resulting in a yield stress and high apparent viscosity in Fig. 5. The particles in the suspension with PEG, on the other hand, dispersed well, even though this suspension also had a yield stress and high apparent viscosity. These

Table 2
Average particle size obtained from direct observation and packing fraction of sediment for centrifugal sedimentation test.

Additive	Average particle size [μm]	Packing fraction [−]
CMC	15.2	0.056
PEG	8.04	–
PEI	9.44	0.152
Non	9.08	0.178

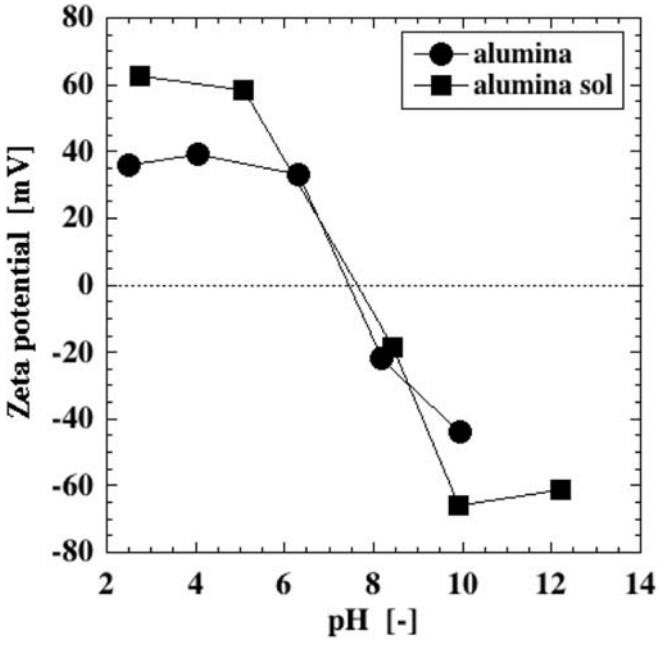

Fig. 8. Zeta potential of alumina powder and inorganic binder sol.

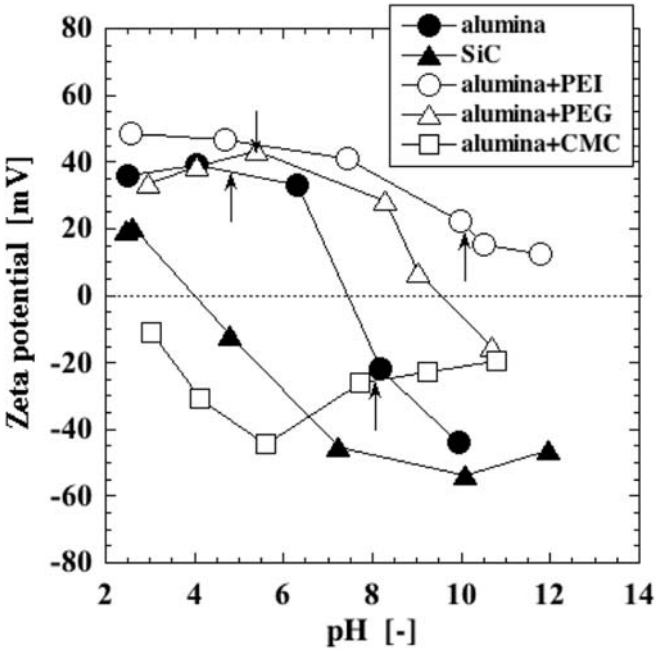

Fig. 9. Zeta potential of alumina powder after addition of each additive, and of SiC substrate (arrows in the figure represent the pH of the suspension after the addition of each additive).

Table 3
Al/Si ratio on the surface.

Additive	Al/Si ratio [−]
CMC	4.64
PEG	0.25
PEI	31.6
Non	2.08

results indicate that the cause of the yield stress and high apparent viscosity should be a bulky network structure of PEG and alumina particles that were still well-dispersed. For the suspension with PEI, which had no yield stress and a quite low apparent viscosity, alumina particles flocculated a little, compared to the suspension without additives.

The final packing fractions of formed sediments are also summarized in Table 2. Comparing the sediment packing fractions, it was found that particles flocculated in the suspension with CMC and flocculated slightly in the suspension with PEI, as mentioned above. The final packing fraction of the formed sediment for the suspension with PEG could not be determined, since the particles dispersed well and the solution viscosity was quite high, resulting in slow settling of the particles. However, this phenomenon did indicate that the particles dispersed well in the suspension with PEG.

Fig. 8 shows the zeta potentials of raw alumina particles and particles in the alumina sol used in this study, showing almost the same trend. Thus, the particle dispersion and flocculation state did not change much after addition of the inorganic binder.

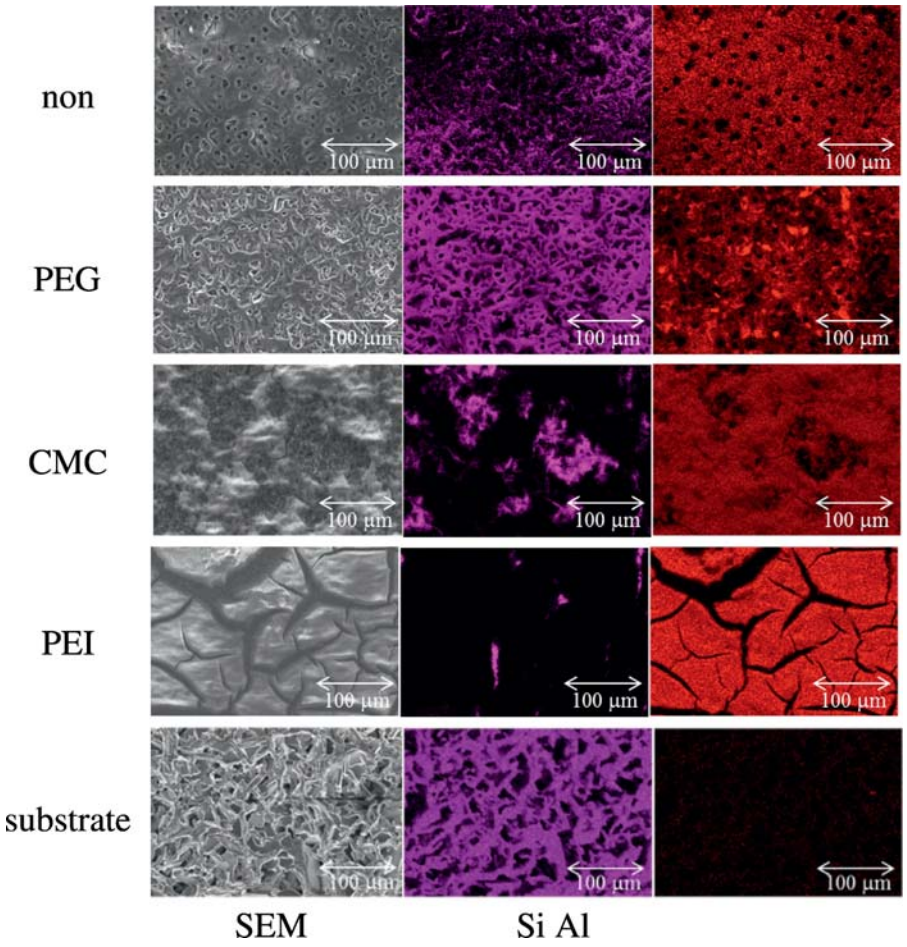

Fig. 10. Scanning electron microscope (SEM) images of the surface of coated porous media and ion mapping of Si and Al.

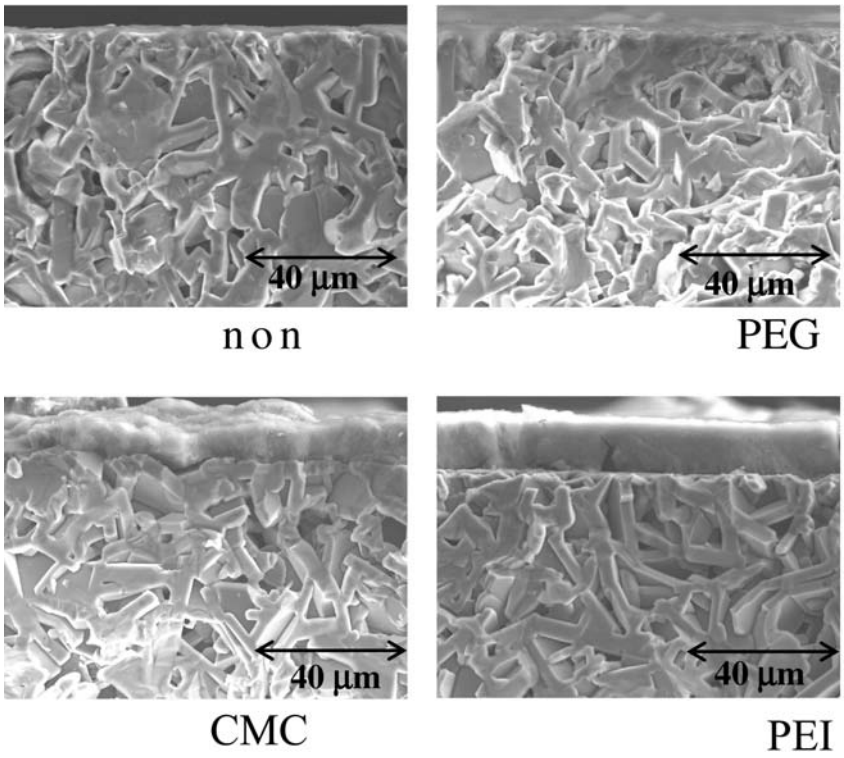

Fig. 11. SEM images of the cross-sections of coated porous media.

Fig. 9 shows the zeta potential of the particles and the suspension pH values after the addition of additives. For the suspension with PEI, the zeta potential of the particles became positive and relatively large (above 40 mV) at pH values from 2.5 to 7.5. For the suspension with CMC, on the other hand, the zeta potential of the particles became negative and relatively large at a pH of about 5.5. For the suspension with PEG, similar as for raw alumina particles, the zeta potential of the particles changed from positive to negative as the pH of the suspension increased, and was relatively large at pH values of 3.0–6.0. From these results, we can see that the particles in the suspension without additives dispersed well because they had a relatively large positive charge. The particles in the suspension with PEG were also well dispersed for the same reason. For the suspension with CMC, on the other hand, particles had a negative charge due to adsorption of the anionic polymer. Combining the results of the flow curve, direct observation, and centrifugal sedimentation of the suspension, the particles likely formed flocs due to CMC bridging among alumina particles. For the suspension with PEI, finally, the surface charge was positive due to adsorption of the cationic polymer PEI. However, the magnitude of this positive charge decreased by shifting the pH value to basic, resulting in flocculation of the particles.

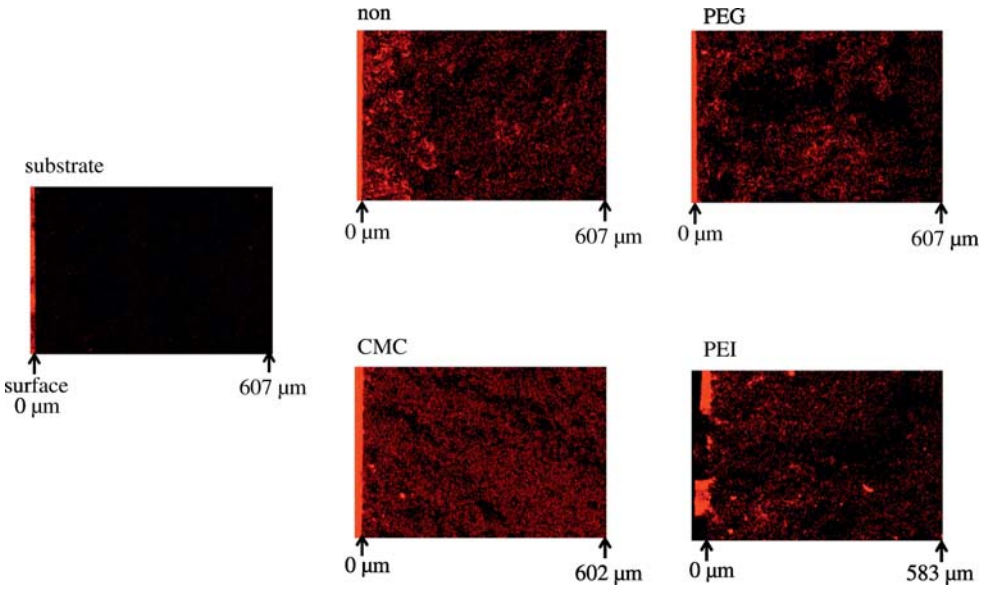

Fig. 12. Al ion mapping of the cross-sections of coated porous media.

3.2. Relationship between coating characterization and suspension characterization

Fig. 10 shows the SEM images and mapping of Si and Al on the surface of the coated substrates. The values for the mass ratio Al/Si are summarized in Table 3. The particles were homogeneously coated for both the suspensions without additives and with PEG; however, when comparing them, more pores were clogged by particles for the suspension without additives, resulting in a higher value for Al/Si. The suspension with PEG yielded the most homogeneous coating among all suspensions used in this study, resulting in the smallest value for Al/Si. The coating fabricated from the suspension with CMC exhibited large aggregates and became an inhomogeneous structure. It was interesting that both the suspensions with PEG and CMC had a yield stress and high apparent viscosities, yet resulted in different coating states. For the suspension with PEI, the surface of the substrate became fully covered by a thick layer of alumina particles, resulting in the highest Al/Si value among all suspensions in Table 4. In addition, many large cracks were observed, suggesting that the larger coating thickness caused crack formation during drying. Fig. 11 and 12 show the SEM images and mapping of Al for the cross-sections of the coated substrates. Fig. 13 also shows the mass ratio distribution of Al at each position of the cross-sections of the coated substrates. The coating thicknesses were quite small, and the interfaces between the coating layers and substrates not clear, for the suspensions without additives and with PEG. For the suspensions with CMC and PEI, on the other hand, the coating thicknesses were relatively large and the interfaces between the coating layers and substrates were clear. In addition, particles penetrated into the pores of the substrate for the suspensions without additives and with PEG, while most particles stayed on and near the surface of the substrate for the suspensions with CMC and PEI.

Fig. 14 shows the changes in air permeation resistance for the substrates before and after coating. An increase in the permeation resistance ratio correlated well with the degree of particle penetration into the pores of the substrates discussed in Fig. 13. In other words, the permeation resistance ratio for the suspension without additives was the greatest, followed by those for suspensions with PEG, PEI, and finally CMC. For the suspension without additives, the particles in the suspension dispersed well, based on direct observation of the particle dispersion state, as shown in Fig. 7 and Table 2. In addition, this suspension was blown off the substrate by spinning less and penetrated the substrate more compared to the suspension with PEG, based on the observations of the suspensions after dropping them onto the substrates. Since the particles in the suspension without additives dispersed well, similar to the suspension with PEG, more particles penetrated the substrate, resulting in the highest permeation resistance. For the suspensions with PEI and CMC, air permeated through large cracks, as shown in Fig. 10. Thus, the permeation resistance did not increase much, even though the coating thickness was large.

Here, the relationship between the coating and suspension characterization results are discussed. Fig. 15 shows a schematic illustration of coating structures obtained from the suspensions with varying additives. In this study, the suspension with PEG yielded the most homogeneous coating, and the amount of particles penetrating into the substrate pores could be suppressed to some extent. The latter occurred as the result of a PEG network structure that effectively prevented penetration. Despite the PEG network structure, particles still dispersed well, thereby forming a homogeneous coating layer. For the suspension without additives, a relatively homogeneous coating could be obtained; however, since a PEG-like network structure did not exist, the particles could penetrate into the pores, resulting in a relatively large increase in the air permeation resistance. Comparing the above results for suspensions without additives and with PEG, it appears to be difficult for particles to stay on and near the surface of the SiC substrates only using electrostatic interactions between the positively-charged alumina particles and negatively-charged substrates.

For the suspension with CMC, the obtained coating was inhomogeneous with large aggregates, even though particle penetration into the substrate pores was suppressed due to particle flocculation in the suspension. The flow curves for the suspensions with PEG and CMC showed very similar trends with yield stresses and high apparent viscosities; however, only the suspension with PEG yielded a homogeneous coating. Direct observation of the particle dispersion states confirmed that particles dispersed well in the suspension with PEG, while particles flocculated in the suspension with CMC. These results indicate that the particle dispersion state needs to be characterized using an appropriate method in order to control the coating microstructure on porous substrates.

For the suspension with PEI, the coating was thick and contained cracks, even though little particle penetration was observed. One of the likely reasons for the large coating thickness is that the suspension

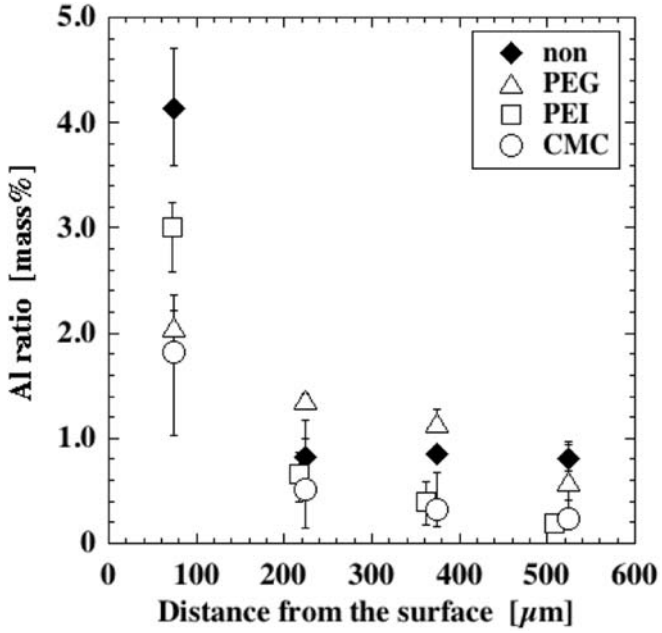

Fig. 13. Change in Al/Si ion ratio of the cross-sections at each distance from the surface.

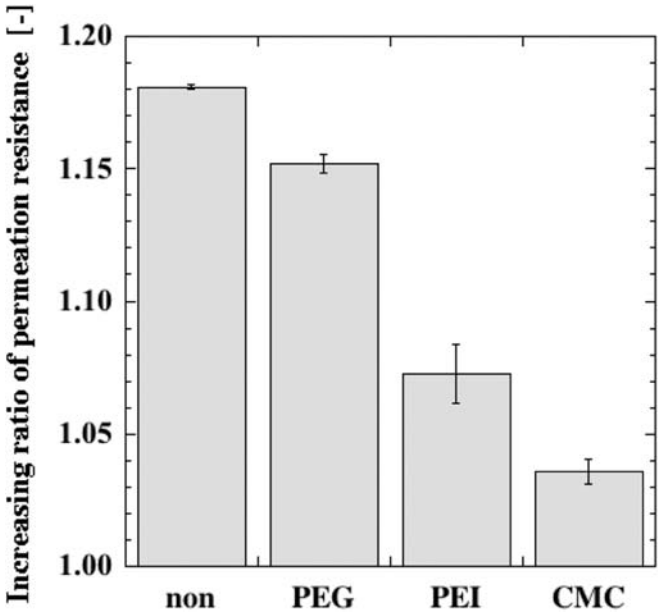

Fig. 14. Increase in ratio of permeation resistance for the coated porous media.

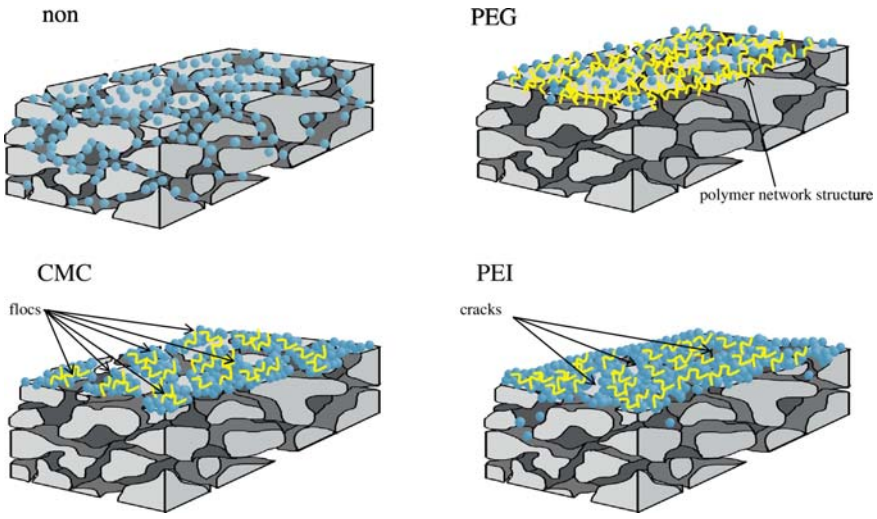

Fig. 15. Schematic illustration of the structure of each coating.

amount on the substrate after spinning was relatively large compared to the suspensions with other additives. In addition, the substrate pores were clogged by weakly flocculated particles caused by the pH shift of the suspension after addition of PEI, resulting in the formation of a thick coated layer. Although the amount of suspension on the substrate is of course adjustable, the pH shift that decreases the magnitude of the surface charge is considered to be difficult to avoid in the suspension with PEI, since PEI is a relatively strong base. The latter suggests that coatings that are more homogeneous than the one with the PEG suspension may be difficult to obtain.

4. Conclusions

Alumina suspensions with different additives were coated onto porous SiC substrates. Comparing the results of both the coating and suspension characterizations, the following conclusions were obtained:

(1) For the suspension with polyethylene glycol (PEG), alumina particles dispersed well in the suspension and the added PEG formed a network structure, resulting in a homogeneous coating on the surface of the substrate with less particle penetration into the substrate pores.
(2) For the suspension with carboxymethyl cellulose (CMC) and the suspension with polyethylenimine (PEI), since particles flocculated in the suspensions, particle penetration into the substrate pores hardly occurred; however, the formed coating was inhomogeneous.

From the above, we can conclude that PEG was the most suitable additive to obtain a homogeneous coating with a relatively low air permeation resistance. In addition, the results also demonstrate that characterization of particle dispersion state in suspensions based on appropriate methods is very important to control their properties for optimally coating porous substrates, since suspensions with almost the same apparent viscosities have completely different particle dispersion states, for example suspensions with PEI and CMC.

Acknowledgement

A part of this research was financially supported by Adaptable and Seamless Technology transfer Program through Target-driven R&D (A-STEP) Stage I, Industry needs response type, “High Performance of Ceramics and Manufacturing Process”, from Japan Science and Technology Agency (JST) (AS282I005e).

References

[1] A.G. Martin, M.P. Orihuela, J.A. Becerra, J.M. Fernandez, J.R. Rico, Permeability and mechanical integrity of porous biomorphic SiC Ceramics for application as hot-gas filters, Mater. Des. 107 (2016) 450–460.
[2] J.M.R. Gallo, G. Gatti, A. Graizzarzo, L. Marchese, H.O. Pastore, Novel mesoporous carbon ceramics composites as electrodes for direct methanol fuel cell, J. Power Sources 196 (2011) 8188–8196.
[3] T. Isobe, M. Shimizu, S. Matsushita, A. Nakazima, Preparation and gas permeability of the surface-modified porous Al_2O_3 ceramic filter for CO_2 gas separation, J. Asian. Ceram. Soc. 1 (2013) 65–70.
[4] G. Parcianello, E. Bernardo, P. Colombo, Cordierite ceramics from silicon resins containing nano-sized oxide particle fillers, Ceram. Int. 39 (2013) 8893–8899.
[5] Y. Nakagoshi, Y. Suzuki, Pseudobrookite-type $MgTi_2O_5$ water purification filter with controlled particle morphology, J. Asian. Ceram. Soc. 3 (2015) 334–338.
[6] V. Paunovic, V. Ordomsky, M. Fernanda, N. D'Angelo, J.C. Schouten, T.A. Nijhuis, Catalyst coating on prefabricated capillary microchannels for the direct synthesis of hydrogen peroxide, Ind. Eng. Chem. Res. 54 (2015) 2919–2929.
[7] C. Zhang, X. Li, H. Ji, X. Sun, Coating on porous Si_3N_4 based substrate with sol-gel slurry, Integr. Ferroelectr. 138 (2012) 111–116.
[8] C. Agrafiotis, A. Tsetsekou, C.J. Stournaras, A. Julbe, L. Dalmazio, C. Guizard, Deposition of nanophase doped-ceria systems on ceramic honeycombs for automotive catalytic applications, Solid State Ionics 136-137 (2000) 1301–1306.
[9] H. Itoh, H. Asano, K. Fukuroi, M. Nagata, H. Iwahara, Spin coating of a $Ca(Ti, Fe)O_3$ dense film on a porous substrate for electrochemical permeation of oxygen, J. Am. Ceram. Soc. 80 (6) (1997) 1359–1365.
[10] M.F.M. Zwinkels, S.G. Jaras, P.G. Menon, Preparation of anchored ceramic coatings on metal substrates: a modified sol-gel technique using colloidal silica sol, J. Mater. Sci. 31 (1996) 6345–6349.
[11] M. Ozawa, K. Araki, Effect of La modification on the stability of coating alumina layer on FeCrAl alloy substrate, Surf. Coat. Technol. 271 (2015) 80–86.
[12] C. Voigt, C.G. Aneziris, J. Hubalkova, Rheological characterization of slurries for the preparation of alumina foams via replica technique, J. Am. Ceram. Soc. 98 (5) (2015) 1460–1463.
[13] C.C. Huang, Y.J. Huang, H.S. Wang, F.G. Tseng, Y.C. Su, A well-dispersed catalyst on porous silicon micro-reformer for enhancing adhesion in the catalyst-coating process, Int. J. Hydrog. Energy 39 (2014) 7753–7764.
[14] C. Agrafiotis, A. Tsetsekou, Deposition of meso-porous γ-alumina coatings on ceramic honeycombs by sol-gel methods, J. Euro. Ceram. Soc. 22 (2002) 423–434.
[15] C. Agrafiotis, A. Tsetsekou, I. Leon, Effect of slurry rheological properties on the coating of ceramic honeycombs with yttria-stabilized-zirconia washcoats, J. Am. Ceram. Soc. 83 (5) (2000) 1033–1038.
[16] J. Tsubaki, M. Kato, M. Miyazawa, T. Kuma, H. Mori, The effects of the concentration of a polymer dispersant on apparent viscosity and sedimentation behavior of dense slurries, Chem. Eng. Sci. 56 (2001) 3021–3026.
[17] T. Athena, C. Agrafiotis, A. Milias, Optimization of the rheological properties of alumina slurries for ceramic processing applications part I: slip-casting, J. Euro. Ceram. Soc. 21 (2001) 363–373.
[18] J.J. Guo, J.A. Lewis, Effect of ammonium chloride on the rheological properties and sedimentation behavior of aqueous silica suspensions, J. Am. Ceram. Soc. 83 (2000) 266–272.
[19] R. Greenwood, E. Roncari, C. Galassi, Preparation of concentrated aqueous alumina suspensions for tape casting, J. Euro. Ceram. Soc. 17 (1997) 1393–1401.
[20] B.V. Velamakanni, J.C. Chang, F.F. Lange, D.S. Pearson, New method for efficient colloidal particle packing via modulation of repulsive lubricating hydration forces, Langmuir 6 (1990) 1323–1325.

[21] K. Asai, K. Naganawa, T. Mori, J. Tsubaki, Direct observation and characterization of effect of preparing condition on particle assembling state in suspension, J. Soc. Powder Technol., Japan 49 (2012) 177–183.
[22] K. Asai, K. Naganawa, T. Mori, J. Tsubaki, Direct observation and characterization of particle assembling state in suspension, J. Soc. Powder Technol., Japan 48 (2011) 518–525.
[23] T. Nakae, Reorojikogaku to Sono Ouyougijyutsup.13 Fuji Technosystem Co., Ltd., 2001
[24] K. Asai, M. Ichiyanagi, H. Satone, T. Mori, J. Tsubaki, Y. Ito, The influence of non-newtonian property on the apparent viscosity measured by single cylinder rotational viscometer (type-B viscometer), J. Soc., Powder Technol., Japan 46 (2009) 873–880.
[25] J. Masliyah, S. Bhattachrjee, Electrokinetic and Colloid Transport Phenomena, Wiley-Interscience, New York, 2006 311–318.